Human Molecular Genetics, 2015, Vol. 24, No. 15 4443–4453

doi: 10.1093/hmg/ddv180
Advance Access Publication Date: 13 May 2015
Original Article

ORIGINAL ARTICLE

Kabuki syndrome genes *KMT2D* and *KDM6A*: functional analyses demonstrate critical roles in craniofacial, heart and brain development

Peter M. Van Laarhoven[1,†], Leif R. Neitzel[1,†], Anita M Quintana[1], Elizabeth A. Geiger[1], Elaine H. Zackai[3], David E. Clouthier[4], Kristin B. Artinger[2,4], Jeffrey E. Ming[3] and Tamim H. Shaikh[1,2,*]

[1]Department of Pediatrics, Section of Clinical Genetics and Metabolism and, [2]Intellectual and Developmental Disabilities Research Center, University of Colorado School of Medicine, Aurora, CO, USA, [3]Division of Human Genetics, Department of Pediatrics, The Children's Hospital of Philadelphia, the University of Pennsylvania School of Medicine, Philadelphia, PA, USA and [4]Department of Craniofacial Biology, University of Colorado Anschutz Medical Campus, Aurora, CO, USA

*To whom correspondence should be addressed at :Department of Pediatrics, University of Colorado Denver, 12800 E. 19th Avenue, Mail Stop 8313, Aurora, CO 80045, USA. Email: tamim.shaikh@ucdenver.edu

Abstract

Kabuki syndrome (KS) is a rare multiple congenital anomaly syndrome characterized by distinctive facial features, global developmental delay, intellectual disability and cardiovascular and musculoskeletal abnormalities. While mutations in *KMT2D* have been identified in a majority of KS patients, a few patients have mutations in *KDM6A*. We analyzed 40 individuals clinically diagnosed with KS for mutations in *KMT2D* and *KDM6A*. Mutations were detected in *KMT2D* in 12 and *KDM6A* in 4 cases, respectively. Observed mutations included single-nucleotide variations and indels leading to frame shifts, nonsense, missense or splice-site alterations. In two cases, we discovered overlapping chromosome X microdeletions containing *KDM6A*. To further elucidate the functional roles of *KMT2D* and *KDM6A*, we knocked down the expression of their orthologs in zebrafish. Following knockdown of *kmt2d* and the two zebrafish paralogs *kdm6a* and *kdm6al*, we analyzed morphants for developmental abnormalities in tissues that are affected in individuals with KS, including craniofacial structures, heart and brain. The *kmt2d* morphants exhibited severe abnormalities in all tissues examined. Although the *kdm6a* and *kdm6al* morphants had similar brain abnormalities, *kdm6a* morphants exhibited craniofacial phenotypes, whereas *kdm6al* morphants had prominent defects in heart development. Our results provide further support for the similar roles of *KMT2D* and *KDM6A* in the etiology of KS by using a vertebrate model organism to provide direct evidence of their roles in the development of organs and tissues affected in KS patients.

Introduction

Kabuki syndrome (KS, OMIM # 147920) is a rare, autosomal dominant multiple congenital anomaly (MCA) syndrome. Patients with KS have a recognizable facial gestalt consisting of long palpebral fissures with eversion of the lower lateral lids, high arched eyebrows with sparse growth along the distal third, low-set and

[†]These authors contributed equally to this work.

Received: February 5, 2015. **Revised:** April 3, 2015. **Accepted:** May 11, 2015

prominent ears, a shortened nasal septum and depressed nasal tip (1,2). Additional features that are frequently associated with KS include intellectual disability (ID, 92%), short stature (83%), persistent fingertip pads (93%) and skeletal abnormalities (92%) (1). The extent of ID may vary from low-normal to severe (1). Microcephaly and structural brain abnormalities including polymicrogyria and atrophy of the cerebellum and brainstem have all been described in KS (3–6). Congenital heart defects (CHDs) may have a prevalence as high as 55% and include both septal defects (atrial or ventricular) and aortic coarctation (1,7–9).

Mutations in *KMT2D* (previously *MLL2*) have been identified in 34–76% of patients with KS (10–15). The *KMT2D* transcript spans 19.4 Kb and codes for a 593-kDa protein product (16). *KMT2D* is a member of the SET-domain-containing family of histone methyltransferases, responsible for tri-methylation of histone H3 at lysine 4 (H3K4me3), an epigenetic mark associated with transcriptionally active genes (17,18). Mutations in *KMT2D* could not be identified in all cases of KS, suggesting that there may be other genes underlying the etiology of disease in a subset of KS patients (10). Recently, six *KMT2D*-mutation-negative KS patients were reported to have deletions or nonsense single-nucleotide variations (SNVs) in *KDM6A* (previously *UTX*), a histone H3 lysine 27 (H3K27)-specific demethylase (19–21). The *KDM6A* transcript is 5.4 Kb and is translated into a 154-kDa protein (16). KDM6A removes the H3K27me3 mark that is associated with gene silencing (22,23). KDM6A associates with KMT2D and several other proteins including RBBP5, DPY30, WDR5, MATR3, ASH2L, NSD1, PAXIP1, NCOA6 and c16orf53, in a complex which is involved in regulating the expression of a wide range of downstream genes (24).

In this study, we report the mutation analysis of *KMT2D* and *KDM6A* in 40 individuals clinically diagnosed with KS. We identified potentially pathogenic mutations in either *KMT2D* or *KDM6A* in 16 cases. Further, we have performed functional analysis of *KMT2D* and *KDM6A* by morpholino antisense oligonucleotide-based knockdown of the expression of their zebrafish orthologs. Our results demonstrate that both genes play similar and critical roles in early vertebrate development, and their reduced expression results in craniofacial, cardiac and brain abnormalities.

Results

Analysis of *KMT2D* and *KDM6A* in KS patients

We screened 40 individuals with a clinical diagnosis of KS for mutations in *KMT2D* and *KDM6A*. Genomic DNA from these individuals was first analyzed for copy number alterations using Affymetrix 500-K SNP arrays. Two female subjects were found to have microdeletions on Chromosome X. Subject 1 had a 3.2-MB deletion at ChrXp11.3 (chrX:43620636-46881568) involving 13 genes and Subject 2 had a 2-Mb deletion (chrX:43620636-45642604) involving 7 genes nested within the larger deletion present in the other patient (Fig. 1A). The region shared between the two deletions contained *KDM6A*, which had recently been

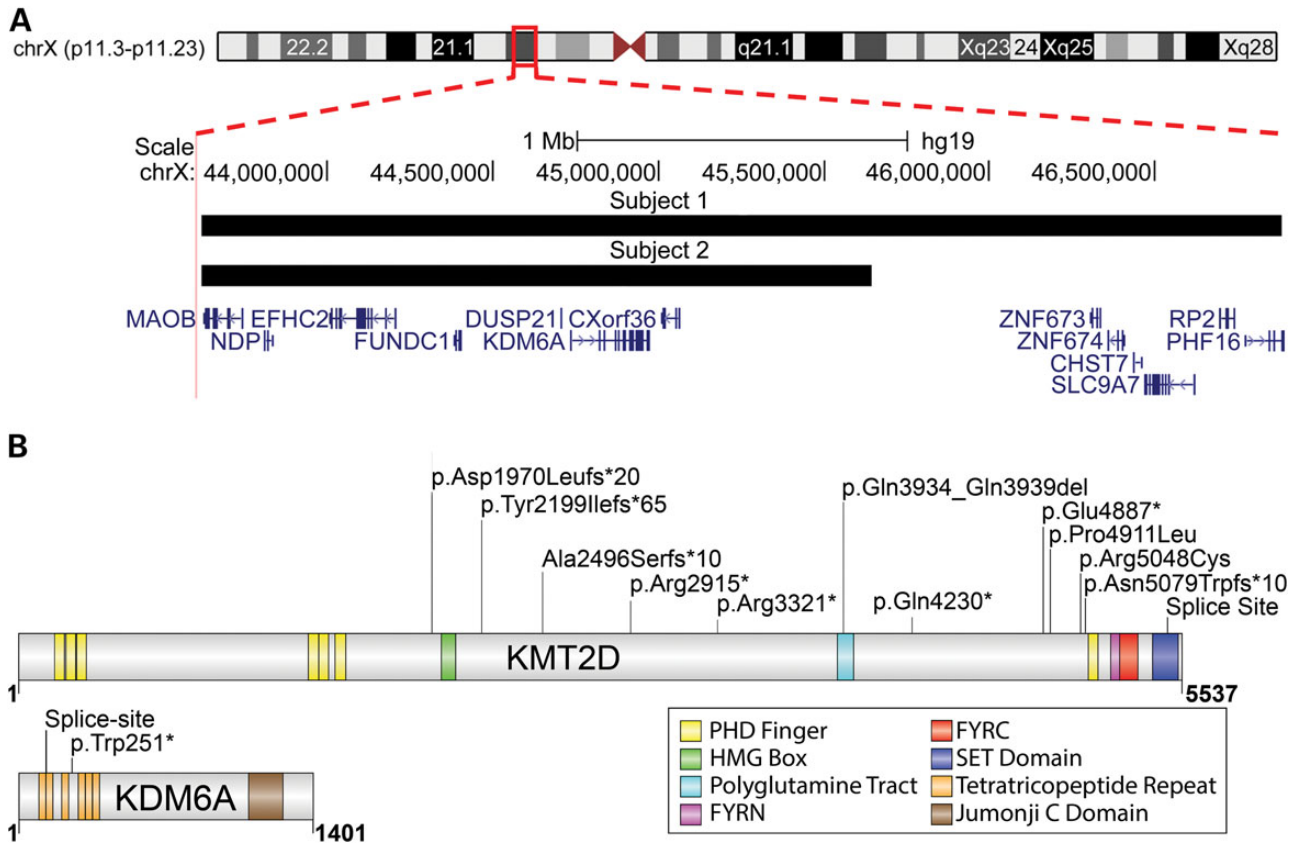

Figure 1. Spectrum of mutations in subjects diagnosed with KS. (**A**) An ideogram of chromosome X is shown, highlighting a region of Xp11.3–p11.23 with a red box. An expanded view of this region is shown including the genes and chromosomal coordinates. The microdeletions detected in Subjects 1 and 2 are shown as black bars. (**B**) The KMT2D and KDM6A proteins are shown as gray bars. The functional domains in each protein are indicated by colored bars. The location of alterations, in both proteins, detected in Subjects 3–16 are indicated by vertical black lines.

Table 1. *KMT2D* and *KDM6A* mutations in KS subjects

Proband	Gender	Gene affected	Chromosomal location (hg19)	Effect at cDNA level	Effect at protein level
1	F	*KDM6A*	chrX:43620636-46881568	Microdeletion	Haploinsufficiency
2	F	*KDM6A*	chrX:43620636-45642604	Microdeletion	Haploinsufficiency
3	F	*KDM6A*	chrX:44913077	c.752G > A	p.Trp251*[1]
4	M	*KDM6A*	chrX:44949177	c.3736 + 2T > C	Splice Site
5	M	*KMT2D*	chr12:49425800	c.12688C > T	p.Gln4230*
6	M	*KMT2D*	chr12:49431178	c.9961C > T	p.Arg3321*
7	F	*KMT2D*	chr12:49432396	c.8743C > T	p.Arg2915*
8	F	*KMT2D*	chr12:49421090	c.14659G > T	p.Glu4887*
9	M	*KMT2D*	chr12:49436066-73	c.5908_5915del	p.Asp1970Leufs*20
10	M	*KMT2D*	chr12:49420511-14	c.15235_15238del	p.Asn5079Trpfs*10
11	M	*KMT2D*	chr12:49434958	c.6595del	p.Tyr2199Ilefs*65
12	F	*KMT2D*	chr12:49434072-73	c.7481dup	p.Ala2496Serfs*10
13	M	*KMT2D*	chr12:49415935	c.16413-1G > C	Splice Site
14	M	*KMT2D*	chr12:49426675–92	c.11796_11813del	p.Gln3934_Gln3939del
15	F	*KMT2D*	chr12:49420607	c.15142C > T	p.Arg5048Cys
16	F	*KMT2D*	chr12:49421017	c.14732C > T	p.Pro4911Leu

F, female; M, male; *, premature stop codon; del, deletion; fs, frame shift; dup, duplication.

shown to be deleted in three *KMT2D*-mutation-negative KS patients (19). Furthermore, no other copy number variations (CNVs) of clinical significance were detected in any of the remaining subjects. We next performed targeted Sanger sequencing of all exons of *KMT2D* and *KDM6A* in all 40 subjects, which detected 2 additional mutations in *KDM6A* and 12 mutations in *KMT2D* (Table 1). The mutations that were detected are described further in the Supplementary Material.

Expression patterns of zebrafish orthologs of *KMT2D* and *KDM6A*

In order to study the potential role of *KMT2D* and *KDM6A* in vertebrate development, we used the zebrafish (*Danio rerio*) as a model organism. There is one ortholog of *KMT2D* (*kmt2d*) in zebrafish, and two orthologs of *KDM6A* (*kdm6a* and *kdm6al*), which arose from an evolutionary partial genome duplication in teleosts (25). We used whole-mount *in-situ* hybridization to determine that *kmt2d*, *kdm6a* and *kdm6al* transcripts are similarly ubiquitously expressed throughout the embryo by 24-h post-fertilization (hpf), with the highest expression observed in the head (Supplementary Material, Fig. S1). By 48 hpf, transcript levels are reduced, but still present in the brain.

Knockdown of *kmt2d*, *kdm6a* and *kdm6al* with morpholino antisense oligonucleotides

We hypothesized that the distinctive craniofacial features observed in KS are predominantly caused by haploinsufficiency of *KMT2D* or *KDM6A* during development. To test this, we designed a combination of transcription start-site (TSS) and splice-site (SS) blocking morpholinos (MOs) to knock down the expression of *kmt2d*, *kdm6a* and *kdm6al*. Embryos were injected with MOs prior to the four-cell stage to knock down the expression of the target genes, after which the developmental progress of the embryos was monitored (26). Efficacy of SS blocking morpholinos was confirmed by reverse transcription PCR and sequencing of transcripts obtained from injected embryos (Supplementary Material, Fig. S2). Translation blocking and SS blocking MOs were injected independently to ensure similar phenotypes were obtained and then combined.

Analysis of craniofacial development in morphants

Alcian blue and alizarin red staining was performed on 5 day post-fertilization (dpf) morphants to visualize cartilage and bone, respectively. In *kmt2d* morphants ($N = 41$), we observed significant craniofacial defects with severe hypoplasia of the viscerocranium as compared with uninjected controls, including complete loss of branchial arches 3–7 (68%), Meckel's cartilage (22%) and the ceratohyal (44%) from the cartilaginous structures, whereas the bony cleithrum (85%) and opercles (42%) were commonly absent as well (Fig. 2A, B and Supplementary Material, Table S1). When these structures were present, they were often incompletely formed or clefted, and in the case of the ceratohyal cartilage joint, inverted in a posterior orientation (Supplementary Material, Table S1). Development of the neurocranium appeared normal, except for a slight truncation of the ethmoid plate and trabeculae. Rescue experiments using human *KMT2D* transcript or the zebrafish ortholog were not possible owing to unavailability of full-length cDNA clones, likely due to the extremely large size of *KMT2D* transcript (>19 Kb).

We observed a craniofacial phenotype comparable with *kmt2d* morphants in the *kdm6a* morphants as well ($N = 131$). This included hypoplastic branchial arches (92%), Meckel's cartilage (18%), ceratohyal (40%), cleithrum (72%) and opercles (87%) at similar levels to *kmt2d* morphants (Fig. 2C and Supplementary Material, Table S1). Coinjection of *kmt2d* MO with *kdm6a* MO was embryonic lethal prior to 4 dpf (data not shown). We also co-injected *kdm6a* MO with *in vitro* synthesized human *KDM6A* transcript ($N = 30$). This led to a partial rescue of the craniofacial phenotype, with a reduced number of embryos missing the branchial arches (13%), Meckel's cartilage (3%), ceratohyal (13%), cleithrum (7%) and opercles (30%), demonstrating that the knockdown of *kdm6a* is causing these specific defects and that the human homolog is sufficient to rescue the morphant phenotype (Fig. 2D and Supplementary Material, Table S1). The *kdm6al* morphant ($N = 31$) did not exhibit craniofacial defects (Fig. 2E and Supplementary Material, Table S1). Co-injection of *kdm6a* and *kdm6al* MO did not alter the severity of the phenotype compared with *kdm6a* morphants alone. Together, these data suggest that both *kmt2d* and *kdm6a* are necessary for patterning of the viscerocranium during embryonic development and that *kdm6al* does not function in this role.

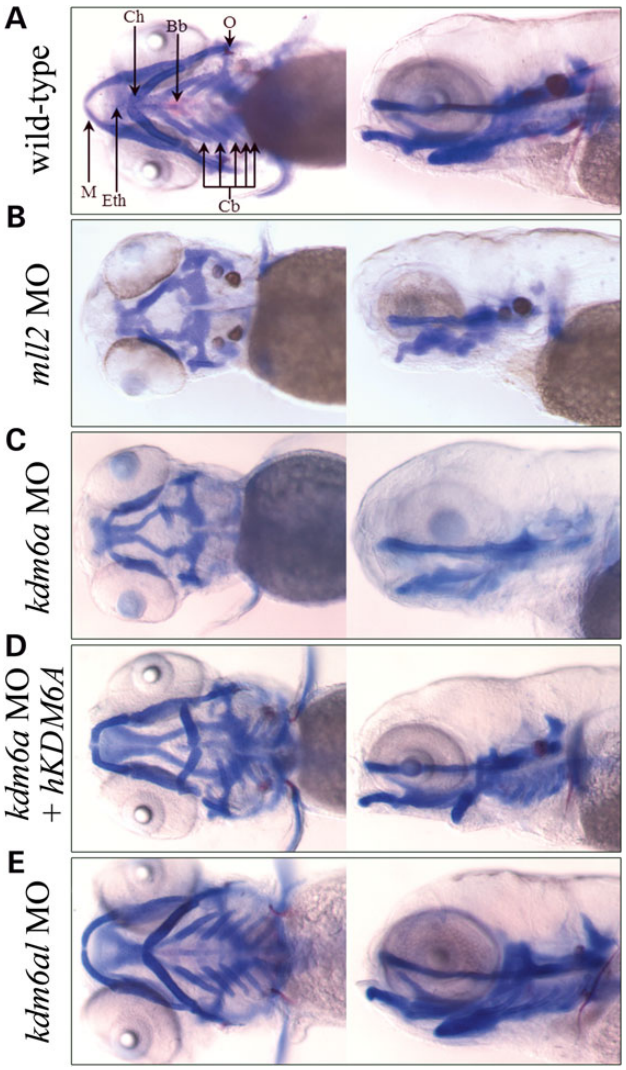

Figure 2. Defects in craniofacial development observed in morphant zebrafish embryos. Five day post-fertilization embryos were treated with alcian and alizarin dyes, which stain cartilage blue and bone red. Both ventral and left sagittal views focused on the visceral cranial cartilages at 10× magnification are shown. (**A**) Un-injected, wild-type control; (**B**) A typical *kmt2d* morphant; (**C**) A typical *kdm6a* morphant; (**D**) A *kdm6a* morphant coinjected with human *KDM6A*; (**E**) A typical *kdm6al* morphant. Bb, basibranchial; Cb, ceratobranchial arches 3–7; Ch, ceratohyal; O, opercle; Eth, ethmoid plate; M, Meckel's cartilage.

Morpholino knockdown of *kdm6al* resulted in a posterior truncation defect (Supplementary Material, Fig. S3). However, posterior development was not affected by knockdown of *kmt2d* or *kdm6a* at concentrations that resulted in craniofacial defects (Supplementary Material, Fig. S3).

Analysis of heart development in morphants

The observation of cardiac edema in all three morphants (Supplementary Material, Fig. S3) suggested abnormalities in cardiac function. Consequently, we tested the effect of *kmt2d*, *kdm6a* and *kdm6al* knockdown on cardiac development in the zebrafish transgenic line Tg(szhand2:mCherry;cmlc2:gfp)^{co10}, which expresses GFP under the *cmlc2* promoter to visualize developing cardiac tissues (27). Following MO knockdown, we observed morphological defects in cardiac development at 48 hpf in *kmt2d* and *kdm6al* morphants, with a milder defect in *kdm6a* morphants. Morphants in all three experimental groups exhibited abnormal development of the atria and/or ventricle, as well as prominent bulging of the myocardial wall. This was most pronounced in the *kmt2d* morphants, whereas effects in *kdm6a* and *kdm6al* morphants were less severe.

Additionally, we observed that the organization of the morphant hearts at 48 hpf was more linearly arranged along the midline when compared with wild-type embryos, whose hearts exhibited the S-shape characteristic of proper looping morphology at this time point. In order to quantify the magnitude of this abnormal cardiac morphology, we measured the extent of cardiac looping involution at 48 hpf. The 'looping angle' was determined by measuring the angle of the atrioventricular junction relative to the mid-sagittal plane (Fig. 3, inset). During normal heart development, the looping angle decreases over time as looping involution progresses and is used as a measure of cardiac maturation (28). At 48hpf, the wild-type embryos had an average atrioventricular angle of 32° ($N = 49$). We found that progression through looping morphogenesis was significantly lower in *kmt2d* morphants (71°, $N = 30$, $P = 1.05 \times 10^{-08}$) and *kdm6al* morphants (54° $N = 50$, $P = 4.17 \times 10^{-05}$) compared with wild type, but not significantly different in *kdm6a* morphants (39° $N = 34$, $P = 0.096$) (Fig. 3). This suggests that progression of cardiac looping involution in morphants is defective compared with wild-type embryos.

To test the redundancy of *kdm6a* and *kdm6al* in cardiac development, embryos were co-injected with MOs targeting both *kdm6a* and *kdm6al* together. This resulted in further impairment of the looping progression to levels approaching *kmt2d* morphants (67° $N = 40$, $P = 7.07 \times 10^{-8}$) (Fig. 3). The cardiac phenotype observed in *kdm6al* morphants was partially rescued by coinjection with human *KDM6A* mRNA (41° $N = 31$, $P = 0.001$) (Fig. 3). Co-injection of human *KDM6A* mRNA did not significantly alter the already mild cardiac phenotype of *kdm6a* morphants (data not shown).These data suggest that *kmt2d* and *kdm6al* have crucial roles in cardiac development and that *kdm6a* and *kdm6al* have some functional redundancy in this role.

Analysis of brain development in morphants

In order to determine the effects of the knockdown of KS genes on brain development, we obtained transverse serial sections of the brains of wild type and morphant embryos at 48 hpf. Sections were stained with hematoxylin and eosin to observe cell morphology, and comparable sections through the hypothalamus, optic tectum and midbrain tegmentum were chosen for direct comparison (Fig. 4). When compared with wild-type embryos, the cross-sectional areas of the brains of morphants were notably reduced (Fig. 4). This phenotype was similar between *kmt2d*, *kdm6a* and *kdm6al* morphants and included a reduced cell layer thickness within the hypothalamus, optic tectum and midbrain tegmentum (Fig. 4B, C and E). Co-injection with *hKDM6A* mRNA resulted in a partially restored cell layer thickness in both *kdm6a* and *kdm6al* morphants (Fig. 4D and F). The hindbrain was not as severely affected in morphant embryos (Supplementary Material, Fig. S4). We observed a reduced cell layer thickness in sections through the hindbrain, including a decrease in the size of the medulla oblongata (Supplementary Material, Fig. S4). The decrease in hindbrain size did not affect the development of the otic vesicles in any of the morpholino injected embryos.

Additionally, we observed unusually elongated nuclei in cells of the midbrain along the ventricle as well as in the central region of the forebrain in all of the morphant embryos that were

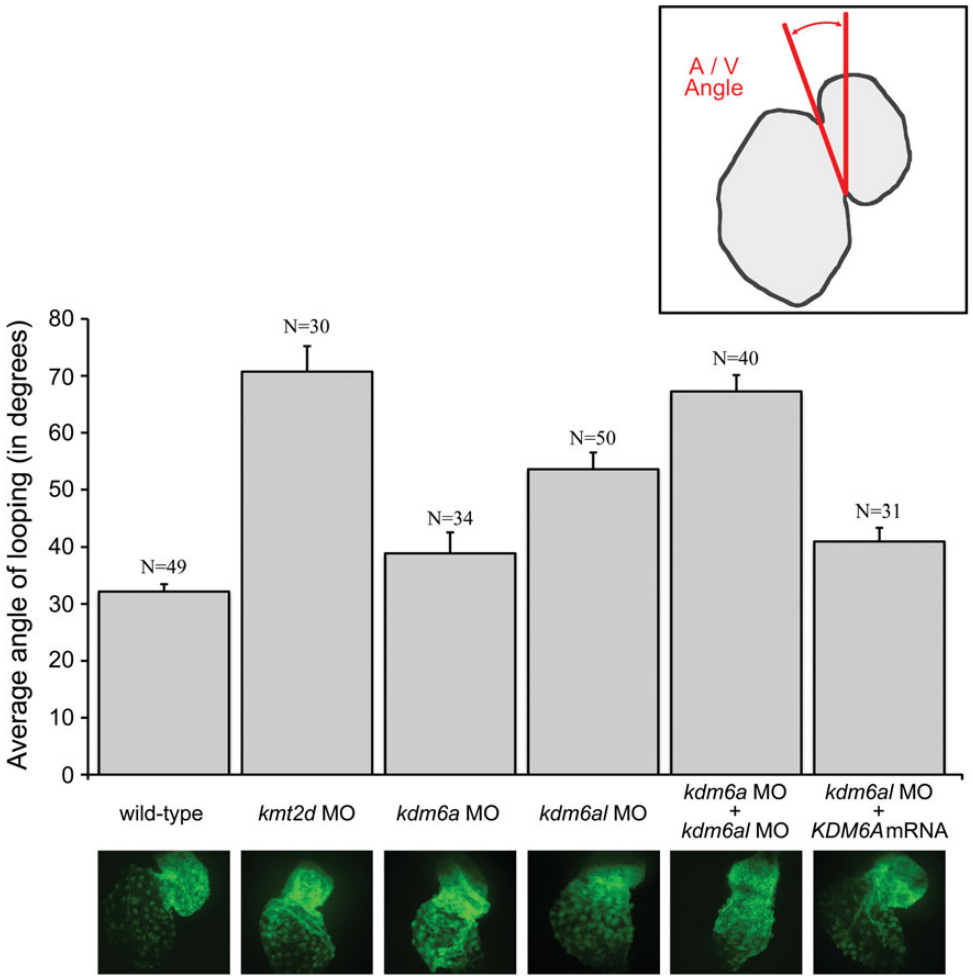

Figure 3. Defects in heart looping observed in morphant zebrafish embryos. Images shown of hearts from 48 h post-fertilization zebrafish embryos in transgenic line Tg (*szhand2*:mCherry; *cmlc2*:gfp)^{co10} which expresses green fluorescent protein (GFP) under the *cmlc2* promoter were analyzed. The looping angle of the heart in the embryos was measured as shown (inset). The measured looping angles are shown as a bar graph for the wild-type and morphant embryos along with a *kdm6al* morphant coinjected with human *KDM6A* mRNA. The number of embryos (*n*) tested in each category are shown. Error bars represent the standard error of the mean. The bottom panel shows representative GFP-expressing hearts from each of the respective categories in the graph.

markedly distinct from the typically rounded nuclei present in wild-type embryos. This phenotype was not observed in the hindbrain sections (Fig. 4 and Supplementary Material, Fig. S4). Within the central nervous system, elongated nuclei are a hallmark of actively dividing neural precursor cells (NPCs) and are not observed in post-differentiated neurons (29). We postulated that a decrease in neuronal differentiation was responsible for the differences between wild-type and morphant brains. We therefore evaluated expression of the NPC marker *sox2* and the post-mitotic neuronal marker *huc* in the brains of an additional series of 48 hpf transverse sectioned embryos (Fig. 5) (29,30). In wild-type embryos, a thin layer of sox2-positive NPCs was observed lining the ventricles of the optic tectum and midbrain tegmentum, and in the central portion of the hypothalamus. The majority of cells in these structures express *huc*, indicating that they have undergone differentiation into early neurons. In contrast, a much larger population of cells within the forebrain and midbrain of *kmt2d*, *kdm6a* and *kdm6al* morphant embryos continue to express *sox2* at this time point. Only a small number of cells express *huc* in the morphants, indicating that NPCs are defective in their ability to differentiate. These differentiation defects were not observed in the hindbrain of morphant embryos (data not shown). These experiments highlight that *kmt2d*, *kdm6a* and *kdm6al* all have essential roles in neuronal differentiation during normal vertebrate brain development.

Discussion

We have screened individuals clinically diagnosed with KS for mutations in the candidate genes *KMT2D* and *KDM6A*. Of the 40 subjects tested, 16 had mutations in either *KMT2D* or *KDM6A*, the two genes identified thus far as causative of KS. All of the variants detected were predicted to be deleterious by computational tools that predict the effect of mutations on protein function. Previous studies have detected *KMT2D* mutations in 44–76% of patients, whereas *KMT2D* mutations were identified in 32% of subjects in this study (10–15). This difference in the detection rate of *KMT2D* mutations in our study is partly due to the fact that 16 of the subjects in our cohort who best fit the 'classic' KS presentation had been previously sequenced for *KMT2D* mutations and are not included in these numbers (11). The majority of these KS subjects (14/16, 88%) carried deleterious mutations in *KMT2D*. KS has a highly variable phenotype, and these results support the suggestion by Banka *et al.* (2011) that patients

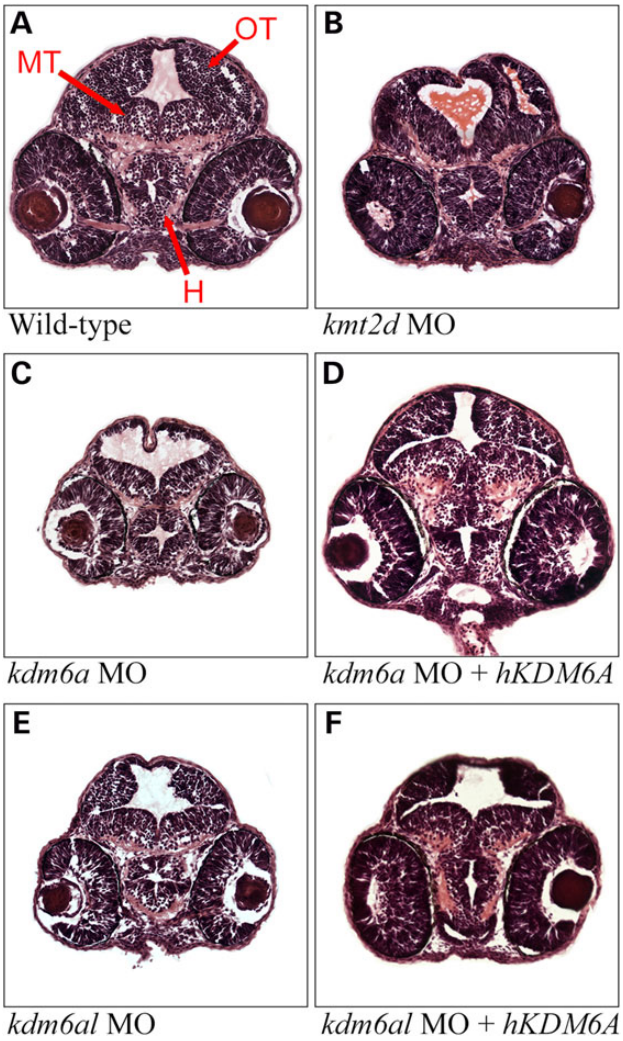

Figure 4. Defects in brain morphology observed in morphant zebrafish embryos. Hematoxylin and eosin (H&E) stained transverse sections of the zebrafish containing elements of both fore- and mid-brain at 48 h post-fertilization. (**A**) Wild-type control, (**B**) a typical *kmt2d* morphant, (**C**) a typical *kdm6a* morphant, (**D**) a typical *kdm6a* morphant coinjected with human *KDM6A* mRNA, (**E**) a typical *kdm6al* morphant and (**F**) a typical *kdm6al* morphant coinjected with human *KDM6A* mRNA. H, hypothalamus; MT, midbrain tegmentum; OT, optic tectum.

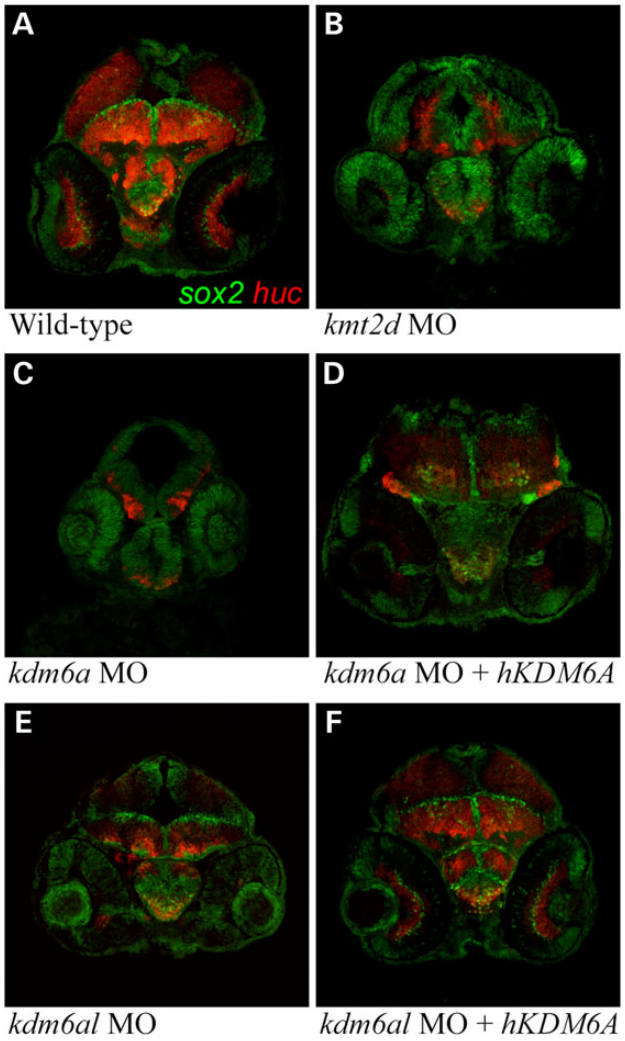

Figure 5. Expression of *sox2* and *huc* in morphant zebrafish embryo brains. Transverse sections through the brain of 48 h post-fertilization zebrafish embryos immunofluorescently labeled with anti-sox2 (green) and anti-huc (red) antibodies. (**A**) Wild-type control, (**B**) a typical *kmt2d* morphant, (**C**) a typical *kdm6a* morphant, (**D**) a typical *kdm6a* morphant coinjected with human *KDM6A* mRNA, (**E**) a typical *kdm6al* morphant and (**F**) a typical *kdm6al* morphant coinjected with human *KDM6A* mRNA.

exhibiting a phenotype closely matching the 'classic' gestalt of facial and other syndromic features are more likely to have mutations in *KMT2D* (14).

The recent discovery of deletions encompassing *KDM6A* in 3/22 (14%) subjects with KS was the first evidence that mutations in a gene other than *KMT2D* can cause the syndrome (19). An additional screen detected point mutations in 3/32 (9%) *KMT2D*-mutation-negative patients, whereas another study failed to find *KDM6A* microdeletions/duplications in a cohort of 120 mutation-negative patients (20,31). Our detection of 4/40 subjects (10%) with variants in *KDM6A* is in accordance with previous findings and indicates that *KDM6A* mutations are not sufficient to explain all of the *KMT2D*-mutation-negative cases of KS. It is noteworthy that *KDM6A* variants were detected in both male and female KS patients in our study and by Lederer *et al.* (19). *KDM6A* has been shown to escape X inactivation independently of the pseudoautosomal regions, suggesting a dosage contribution from both alleles in females (32). Furthermore, *UTY*, the *KDM6A* paralog on the Y chromosome, compensates for the reduced *KDM6A* transcript abundance in males (33). This supports the view that *KDM6A* deletions and mutations, in both males and females, represent an X-linked dominant inheritance.

Subsequently, 24 of our suspected KS subjects did not carry detectable mutations in either *KMT2D* or *KDM6A*. There are multiple possible explanations for this result. One possibility is that some of the mutation-negative subjects have disorders other than KS, but with phenotypes similar to KS patients. Mutations in the *KMT2D*-related histone methyltransferase *KMT2A* have been identified in subjects with Wiedemann–Steiner syndrome, which can be mistaken for KS owing to some phenotypic overlap (34,35). This may explain a small number of cases but is unlikely to be the case in all of these subjects. Another possibility is that mutations in regulatory regions of *KMT2D* and *KDM6A* may account for some of the cases and were not detected by the methods used. The dominant inheritance of KS combined with the types of mutations identified to date makes this less likely.

Alternatively, there may be one or more additional KS causing genes that have not yet been discovered. This possibility is supported by the fact that in the majority of *KMT2D*-mutation-negative patients, a mutation in *KDM6A* is not identified. Many of these patients have 'classic' presentations and yet do not have mutations in either *KMT2D* or *KDM6A*. In addition, both KDM6A and KMT2D carry out their regulatory functions as part of a large protein complex containing several proteins, making them potential candidates for future analysis in mutation-negative cases (24). We are currently utilizing whole-exome sequencing of *KMT2D* and *KDM6A* mutation-negative patients to determine the identity of additional candidate KS genes.

The fact that modifiers of histone methylation are responsible for KS highlights an emerging trend in the genetics of MCA syndromes. There are increasing number of MCA syndromes that appear to result from aberrations in histone modifications or remodeling. These include MCA and IDD disorders associated with mutations in both histone methyltransferases [Sotos syndrome (*NSD1*), Wolf-Hirschhorn syndrome (*NSD2*), 9q sub-telomeric deletion syndrome (*EHMT1*)] and demethylases [X-linked intellectual disability and cleft palate (*PFH8*)] (36–39). Further, CHARGE syndrome (Coloboma, Heart defects, Atresia of the choanae, Retarded growth and development, Genital hypoplasia, Ear anomalies) (40–42) is primarily caused by mutations in *CHD7*, a DNA helicase involved in histone remodeling. CHD7 contains two chromodomains that target its binding and remodeling activity to methylated H3K4, suggesting that development may be impaired owing to disruptions in H3K4 methylation and chromatin remodeling pathways.

Although mutations in *KMT2D* are clearly responsible for the majority of cases of KS, its function in many developmental processes has not been characterized until now. We utilized the zebrafish as a model organism for functional studies of these candidate disease genes, which is an excellent and cost-effective alternative to other vertebrate model organisms such as the mouse. We have used morpholino-based knockdown of *kmt2d, kdm6a* and *kdm6al* in zebrafish to study their roles in the development of structures that are affected in subjects with KS. *KMT2D* activity is required for activation of retinoic acid responsive genes, implicating an important role in regulation of anterior-posterior patterning of the brain (43,44). Furthermore, both *KMT2D* and *KDM6A* have been shown to regulate expression of a number of Hox genes required for body patterning during development (45–47). The *kdm6a* and *kdm6al* genes have been knocked down in zebrafish previously. A reduced posterior body length and abnormal curvature of the spine has been reported in both *kdm6a* and *kdm6al* morphants, with misexpression of Hox genes and notochord degeneration (48). This may be related to spinal cord defects that are observed in some KS subjects, such as scoliosis (35%) and spina bifida occulta (19%) (49). This phenotype was observed in our *kdm6al* morphants as well, but was not observed in *kmt2d* or *kdm6a* morphants. A more recent study performed a detailed expression analysis of *kdm6a* in zebrafish embryos and demonstrated that knockdown of *kdm6a* led to craniofacial defects similar to those observed in our morphants (50). However, a similar role for *kmt2d* in craniofacial development has not been demonstrated until now.

Knockdown of *kmt2d* and *kdm6a* lead to nearly identical craniofacial defects, most notably hypoplasia of cartilaginous structures of the viscerocranium. Similarly, both *kmt2d* and *kdm6al* were required for proper cardiac looping morphogenesis, with a smaller contribution from *kdm6a*. The distinct roles of *kdm6a* in craniofacial development and *kdm6al* in cardiac development suggest that their functions have diverged since the ancestral gene was duplicated in the teleost lineage. Notably, both paralogs appear to be involved in neuronal development, as knockdown of either *kmt2d*, *kdm6a* or *kdm6al* is sufficient to induce a reduction in brain size and a reduced population of post-mitotic neurons at 48 hpf. This reduced brain volume is similar to clinical microcephaly reported in as many as 25% of KS subjects (49). Although there was an accumulation of neural precursors compared with wild-type embryos, the overall brain size of morphants was considerably reduced. The capacity of human *KDM6A* mRNA to partially rescue the defects caused by knocking down *kdm6a* or *kdm6al* demonstrates a high level of functional conservation between the human and zebrafish proteins. Our data provide the first direct evidence of the overlapping, functional roles of *KMT2D* and *KDM6A* in the development of tissues and organs affected in KS subjects.

Many aspects of the KS phenotype appear to be related to a global growth and developmental delay, including small stature and microcephaly. In the zebrafish, the knockdown of *kmt2d*, *kdm6a* and *kdm6al* lead to incomplete cardiac involution and reduced hindbrain size, both of which may result from global underdevelopment. However, the other defects we observed do not appear to be due to global underdevelopment but are likely due to perturbations in the development of specific tissues, resulting from cellular dysfunction. For example, morphants exhibit hypoplasia of structures that make up the viscerocranium, but not the neurocranium. The viscerocranium is derived from neural crest cells, whereas the neurocranium is mesodermal in origin, suggesting that neural crest derivatives may be specifically affected by haploinsufficiency of KS genes (51,52). Similarly, in the morphants, there is a defect in the differentiation NPCs only within the forebrain and midbrain, but not the hindbrain. Further, even though all morphants have markedly smaller brains, only the kdm6al morphants were reduced in overall body size (Supplementary Material, Fig. S3). Therefore, the defects in brain size in kmt2d and kdm6a morphants are likely a consequence of cellular dysfunction and not the result of underdevelopment. Furthermore, the divergence in the functional roles of kdm6a and kdm6al in the zebrafish suggests that these genes have specific regulatory roles in patterning of the craniofacial skeleton and body axis, respectively.

In summary, we have identified 16 additional mutations in the 2 known candidate genes, *KMT2D* and *KDM6A*, in patients with KS. We have further demonstrated the critical functional roles of these two candidate genes in embryonic development, using zebrafish as a model organism. We determined that knockdown of the zebrafish homologs of *KMT2D* and *KDM6A* causes defects in tissues commonly affected in patients with KS, including structures of the viscerocranial skeleton, heart and brain. We also determined that in some tissues, these genes have overlapping yet distinct functions. Thus, we provide a pathway by which candidate genes identified in subjects with genetically heterogeneous disorders such as KS can be functionally tested through biologically relevant experimentation.

Materials and Methods

Human subjects

All human subject samples used in this study were collected after obtaining informed consent. Subjects were enrolled into an IRB approved research protocol at the Children's Hospital of Philadelphia. All subjects received a clinical diagnosis of KS based on dysmorphic features characteristic of the disorder. Additional clinical features in these subjects included defects in other organ systems associated with KS, including congenital heart disease (aortic

stenosis, ventricular septal defect and atrial septal defect), mild–moderate developmental delay, hypotonia, gastrointestinal abnormalities (gastroesophageal reflux), strabismus, hearing loss, genitourinary abnormalities (vesico-ureteral reflux) and microcephaly. Genomic DNA was obtained either from peripheral blood lymphocytes (PBLs) or from subject-derived cell lines.

Copy number analysis and Sanger sequencing

High resolution copy number analysis was performed using SNP 500 K arrays from Affymetrix (Santa Clara, CA, USA) as previously described (53). PCR amplification of the *KMT2D* and *KDM6A* genes was performed on an Applied Biosystems Veriti 96-well thermal cycler using previously published *KMT2D* primers and primers designed to tile across all exons of *KDM6A* (Supplementary Material, Table S2) (10). Amplicons were purified using SPRI beads and sequenced on an ABI PRISM 3730xl using BigDye Terminator v3.1 chemistry by Beckman–Coulter Genomics (Danvers, MA, USA). Alignment to the reference genes and variant calling was performed using CodonCode Aligner (CodonCode Corporation, Centerville, MA, USA), and all variants were visually inspected for quality. Additional PCR primers were designed and used to amplify regions with low-sequence, quality or low coverage calls for variant confirmation. Identified variants were submitted to ClinVar under accession numbers SCV000207387–SCV000207402.

Zebrafish transgenic strains and husbandry

Zebrafish were raised in the University of Colorado Zebrafish Core Facility as described (54). We used AB/TL wild-type zebrafish, with results reproduced in the Ekkwill line. The $tp53^{zdf1/zdf1}$ transgenic line was used as a control to rule out effects of apoptosis on phenotypes (55,56). Visualization of cardiac structures was accomplished utilizing the Tg(*szhand2:mCherry*; *cmlc2:GFP*)^{co10} transgenic line (27). Embryos collected from pair matings were maintained in E3 medium with 0.00001% (w/v) Methylene Blue (embryo media).

Antisense morpholino and mRNA injections

All Morpholinos were acquired from Gene Tools LLC (Philomath, OR, USA). One TSS blocking antisense MO was developed per gene for *kmt2d* (5′ CGCAGTTTGATTTCTGCTCGTCCAT 3′), *kdm6a* (5′ CCGACACTCCGCACGATTTCATAGA 3′) and *kdm6al* (5′ CCACC GACACTCGGCACGGCTTCAT 3′). Two SS blocking MOs were developed for *kmt2d* (SS1: 5′ GGTATAGCAGCAATGACAAACCATT 3′, SS2: 5′ GGTCCCTAAAATGAGACAACAGCTC 3′) and one was developed for *kdm6a* (5′ GTGTGCTGCAAATAGAGGACAACAC 3′) and *kdm6al* (5′ TTTCCACAAGCATCTTTACCTTCAC 3′). Morpholinos were mixed with a 10 mg/ml Dextran dye (Invitrogen, Grand Island, NY, USA)/0.04 M KCL solution at a 1:1 ratio. 3 nL of MO mixture was injected into the yolk of embryos at the 1–4 cell stage, whereas 1-nL injections were used for mRNA rescue directly into the single-cell zygote using a PLI-100 Pico-Injector from Harvard Apparatus (Holliston, MA, USA). Poorly injected embryos were removed by sorting at 24 hpf for even distribution of fluorescent Dextran dye under a dissecting microscope. Injection of MOs into the $tp53^{zdf1/zdf1}$ strain was performed to control for off-target effects (55). TSS and SS MOs were injected independently to ensure similar phenotypes were obtained before co-injection with sub-phenotypic concentrations of TSS and SS Morpholino in combination. A mixture of 3 ng of each *kmt2d* MO was used to knock down *kmt2d*. *Kdm6a* was knocked down with 6 ng of the TSS and 3 ng of the SS MO, whereas the *kdm6al* injection mixture contained 5 ng each of the TSS and SS MOs. Ten nanograms of standard control MO (5′ CCTCTTACCTCAGTTACAATTTATA 3′) were injected as a control. Co-injection with 4 ng of the *Danio rerio p53* MO (5′ GCGCCATTGCTTTGCAAGAATTG 3′) was used as a control when transgenic lines were used. At no time was more than 3 nL injected into any embryo (26). Rescue experiments were performed by injecting 300 pg of human *KDM6A* mRNA directly into the single cell. The human *KDM6A* mRNA was derived from a full-length cDNA clone obtained from Open Biosystems (Lafayette, CO, USA). *In vitro* transcription was performed with the mMESSAGE mMACHINE SP6 Kit (Invitrogen). We verified the efficacy of SS Morpholinos by RT–PCR (Supplementary Methods and Supplementary Material, Fig. S2).

Phenotyping of morphants

Alcian blue and alizarin red staining was performed as previously described on 5 dpf wild-type and morphant embryos (57). Morphants were scored for loss of craniofacial structures or dysmorphic features, and statistical analysis of phenotypes was carried out using Welch's t-test or the Fisher's exact test in R (Supplementary Material, Table S2). Cardiac phenotypes of morphant and wild-type embryos were assessed in Tg(*szhand2:mCherry;cmlc2:GFP*)^{co10} transgenic embryos, and the looping angle was quantified as previously described (28). To determine brain phenotypes, 48 hpf embryos were embedded head-down in a heated solution consisting of 1.5% Agar and 5% Sucrose in 0.4 M phosphate buffer pH 7.4 and cut into blocks. Blocks were sunk overnight at 4°C in a 30% sucrose solution prepared with 0.1 M phosphate buffer pH 7.4. Transverse sections were obtained from frozen blocks at 7 µm of thickness for H&E staining and 15 µm of thickness for immunofluorescence on an Leica CM 1950 cryostat (Leica Biosystems, Nussloch, Germany). Hematoxylin and eosin (H&E) staining was performed as previously described. For cryosection immunofluorescence, samples were rehydrated for 30 min in PBS, blocked for 30 min in PBS supplemented with 5% BSA and 5% goat serum, incubated overnight at 4°C with primary antibodies in blocking solution, washed for 45 min with PBS, incubated for 30 min in secondary antibodies in blocking solution, washed for 45 min with PBS and coverslipped with Vectashield mounting media (Vector Laboratories). Antibodies used were rabbit anti-SOX2 (Abcam), mouse anti-*HuC* (Life technologies), AlexaFluor 488 goat anti-rabbit (Life technologies) and AlexaFluor 594 goat anti-mouse (Life technologies).

Imaging

Imaging experiments were performed in the University of Colorado Anschutz Medical Campus Advance Light Microscopy Core. Full-body imaging was performed on a Zeiss dissecting scope equipped with the QIClick imaging system (QImaging, Surrey, BC, USA). Imaging of the heart and brain was performed on a 3I VIVO Upright Spinning Disk confocal from Zeiss (Oberkochen, Germany). Slidebook Imaging software version 5 (Intelligent Imaging Innovations, Denver, CO, USA) was utilized to capture images and for Z-stack compression. Image J version 1.44 (NIH, Bethesda, MD, USA) and Photoshop (Adobe Systems, San Jose, CA, USA) were utilized for image manipulation including brightness, contrast and false coloring.

Web Resources

The URLs for data presented herein are as follows:

dbSNP: http://www.ncbi.nlm.nih.gov/projects/SNP/

Exome Variant Server: http://evs.gs.washington.edu/EVS/
GERP: http://mendel.stanford.edu/SidowLab/downloads/gerp/index.html
MaxEntScan: http://genes.mit.edu/burgelab/maxent/Xmaxentscan_scoreseq.html
PolyPhen-2: http://genetics.bwh.harvard.edu/pph2/
Provean: http://provean.jcvi.org/index.php
SeattleSeq: http://snp.gs.washington.edu/SeattleSeqAnnotation134/
UCSC Genome Browser: http://genome.ucsc.edu/
ClinVar: http://www.ncbi.nlm.nih.gov/clinvar/

Supplementary Material

Supplementary Material is available at *HMG* online.

Acknowledgements

We are grateful to the patients and their families for their participation in this study. We thank Morgan Singleton and Michelle Tellez for excellent zebrafish care and for technical help. Thanks to Bruce Appel for sharing equipment and for valuable discussions, Debbie Garrity for help with cardiac phenotyping, Laura Hernandez-Lagunas and Kristi Lamonica for their technical help and for valuable discussions, and Michael Bamshad and Katy Buckingham for sharing *KMT2D* PCR conditions and primer sequences.

Conflict of Interest statement. None declared.

Funding

This work was supported in part by funds from a grant to T.H.S by the National Institutes of Health (GM081519), funds and services from the Colorado Intellectual and Developmental Disabilities Research Center, and a P30 Zebrafish Core grant (NS5048154). The University of Colorado Anschutz Medical Campus Advance Light Microscopy Core is supported in part by an NIH/NCRR Colorado CTSI Grant (UL1 RR025780). J.E.M. was supported in part by a grant from the Penn Genomics Institute.

References

1. Niikawa, N., Kuroki, Y., Kajii, T., Matsuura, N., Ishikiriyama, S., Tonoki, H., Ishikawa, N., Yamada, Y., Fujita, M. and Umemoto, H. (1988) Kabuki make-up (Niikawa-Kuroki) syndrome: a study of 62 patients. *Am. J. Med. Genet.*, **31**, 565–589.
2. Adam, M. and Hudgins, L. (2005) Kabuki syndrome: a review. *Clin. Genet.*, **67**, 209–219.
3. Ciprero, K.L., Clayton-Smith, J., Donnai, D., Zimmerman, R.A., Zackai, E.H. and Ming, J.E. (2005) Symptomatic Chiari I malformation in Kabuki syndrome. *Am. J. Med. Genet.*, **132**, 273–275.
4. Yano, S., Matsuishi, T., Yoshino, M., Kato, H. and Kojima, K. (1997) Cerebellar and brainstem 'atrophy' in a patient with Kabuki make-up syndrome. *Am. J. Med. Genet.*, **71**, 486–487.
5. Takano, T., Matsuwake, K., Yoshioka, S. and Takeuchi, Y. (2010) Congenital polymicrogyria including the perisylvian region in early childhood. *Congenit. Anom. (Kyoto)*, **50**, 64–67.
6. Di Gennaro, G., Condoluci, C., Casali, C., Ciccarelli, O. and Albertini, G. (1999) Epilepsy and polymicrogyria in Kabuki make-up (Niikawa-Kuroki) syndrome. *Pediatr. Neurol.*, **21**, 566–568.
7. Kawame, H., Hannibal, M.C., Hudgins, L. and Pagon, R.A. (1999) Phenotypic spectrum and management issues in Kabuki syndrome. *J. Pediatr.*, **134**, 480–485.
8. Hughes, H.E. and Davies, S.J. (1994) Coarctation of the aorta in Kabuki syndrome. *Arch. Dis. Child.*, **70**, 512–514.
9. Armstrong, L., Moneim, A.A.E., Aleck, K., Aughton, D.J., Baumann, C., Braddock, S.R., Gillessen-Kaesbach, G., Graham, J.M., Grebe, T. A., Gripp, K.W. *et al.* (2005) Further delineation of Kabuki syndrome in 48 well-defined new individuals. *Am. J. Med. Genet.*, **132**, 265–272.
10. Ng, S.B., Bigham, A.W., Buckingham, K.J., Hannibal, M.C., McMillin, M.J., Gildersleeve, H.I., Beck, A.E., Tabor, H.K., Cooper, G.M., Mefford, H.C. *et al.* (2010) Exome sequencing identifies MLL2 mutations as a cause of Kabuki syndrome. *Nat. Genet*, **42**, 790–793.
11. Hannibal, M.C., Buckingham, K.J., Ng, S.B., Ming, J.E., Beck, A.E., McMillin, M.J., Gildersleeve, H.I., Bigham, A.W., Tabor, H.K., Mefford, H.C. *et al.* (2011) Spectrum of MLL2 (ALR) mutations in 110 cases of Kabuki syndrome. *Am. J. Med. Genet.*, **155**, 1511–1516.
12. Micale, L., Augello, B., Fusco, C., Selicorni, A., Loviglio, M.N., Silengo, M., Reymond, A., Gumiero, B., Zucchetti, F., D'Addetta, E.V. *et al.* (2011) Mutation spectrum of MLL2 in a cohort of kabuki syndrome patients. *Orphanet J. Rare Dis.*, **6**, 38–45.
13. Micale, L., Augello, B., Maffeo, C., Selicorni, A., Zucchetti, F., Fusco, C., De Nittis, P., Pellico, M.T., Mandriani, B., Fischetto, R. *et al.* (2014) Molecular analysis, pathogenic mechanisms, and read through therapy on a large cohort of kabuki syndrome patients. *Hum. Mutat.*, **35**, 841–850.
14. Banka, S., Veeramachaneni, R., Reardon, W., Howard, E., Bunstone, S., Ragge, N., Parker, M.J., Crow, Y.J., Kerr, B., Kingston, H. *et al.* (2011) How genetically heterogeneous is Kabuki syndrome?: MLL2 testing in 116 patients, review and analyses of mutation and phenotypic spectrum. *Eur. J. Hum. Genet.*, **20**, 381–388.
15. Paulussen, A.D.C., Stegmann, A.P.A., Blok, M.J., Tserpelis, D., Posma-Velter, C., Detisch, Y., Smeets, E.E.J.G.L., Wagemans, A., Schrander, J.J.P., van den Boogaard, M.-J.H. *et al.* (2011) MLL2 mutation spectrum in 45 patients with Kabuki syndrome. *Hum. Mutat.*, **32**, 2018–2025.
16. Flicek, P., Amode, M.R., Barrell, D., Beal, K., Billis, K., Brent, S., Carvalho-Silva, D., Clapham, P., Coates, G., Fitzgerald, S. *et al.* (2014) Ensembl 2014. *Nucl. Acids Res.*, **42**, 749–755.
17. Smith, E., Lin, C. and Shilatifard, A. (2011) The super elongation complex (SEC) and MLL in development and disease. *Genes Dev.*, **25**, 661–672.
18. Martin, C. and Zhang, Y. (2005) The diverse functions of histone lysine methylation. *Nat. Rev. Mol. Cell Biol.*, **6**, 838–849.
19. Lederer, D., Grisart, B., Digilio, M.C., Benoit, V., Crespin, M., Ghariani, S.C., Maystadt, I., Dallapiccola, B. and Verellen-Dumoulin, C. (2012) Deletion of KDM6A, a histone demethylase interacting with MLL2, in three patients with kabuki syndrome. *Am. J. Hum. Genet.*, **90**, 119–124.
20. Miyake, N., Mizuno, S., Okamoto, N., Ohashi, H., Shiina, M., Ogata, K., Tsurusaki, Y., Nakashima, M., Saitsu, H., Niikawa, N. *et al.* (2013) KDM6A point mutations cause kabuki syndrome. *Hum. Mutat.*, **34**, 108–110.
21. Hong, S., Cho, Y.-W., Yu, L.-R., Yu, H., Veenstra, T.D. and Ge, K. (2007) Identification of JmjC domain-containing UTX and JMJD3 as histone H3 lysine 27 demethylases. *Proc. Natl Acad. Sci. USA*, **104**, 18439–18444.
22. Hubner, M.R. and Spector, D.L. (2011) Role of H3K27 demethylases Jmjd3 and UTX in transcriptional regulation. *Cold Spring Harb. Symp. Quant.Biol.*, **75**, 43–49.

23. Margueron, R. and Reinberg, D. (2011) The polycomb complex PRC2 and its mark in life. *Nature*, **469**, 343–349.
24. Issaeva, I., Zonis, Y., Rozovskaia, T., Orlovsky, K., Croce, C.M., Nakamura, T., Mazo, A., Eisenbach, L. and Canaani, E. (2007) Knockdown of ALR (MLL2) reveals ALR target genes and leads to alterations in cell adhesion and growth. *Mol. Cell. Biol.*, **27**, 1889–1903.
25. Meyer, A. and Van de Peer, Y. (2005) From 2R to 3R: evidence for a fish-specific genome duplication (FSGD). *Bioessays*, **27**, 937–945.
26. Bill, B.R., Petzold, A.M., Clark, K.J., Schimmenti, L.A. and Ekker, S.C. (2009) A primer for morpholino use in zebrafish. *Zebrafish*, **6**, 69–77.
27. Iklé, J.M., Artinger, K.B. and Clouthier, D.E. (2012) Identification and characterization of the zebrafish pharyngeal arch-specific enhancer for the basic helix-loop-helix transcription factor Hand2. *Dev. Biol.*, **368**, 118–126.
28. Chernyavskaya, Y., Ebert, A.M., Milligan, E. and Garrity, D.M. (2012) Voltage-gated calcium channel CACNB2 (β2.1) protein is required in the heart for control of cell proliferation and heart tube integrity. *Dev. Dyn.*, **241**, 648–662.
29. Gaete, M., Muñoz, R., Sánchez, N., Tampe, R., Moreno, M., Contreras, E.G., Lee-Liu, D. and Larraín, J. (2012) Spinal cord regeneration in Xenopus tadpoles proceeds through activation of Sox2-positive cells. *Neural Dev.*, **7**, 13–29.
30. Park, H.C., Kim, C.H., Bae, Y.K., Yeo, S.Y., Kim, S.H., Hong, S.K., Shin, J., Yoo, K.W., Hibi, M., Hirano, T. *et al.* (2000) Analysis of upstream elements in the HuC promoter leads to the establishment of transgenic zebrafish with fluorescent neurons. *Dev. Biol.*, **227**, 279–293.
31. Priolo, M., Micale, L., Augello, B., Fusco, C., Zucchetti, F., Prontera, P., Paduano, V., Biamino, E., Selicorni, A., Mammì, C. *et al.* (2012) Absence of deletion and duplication of MLL2 and KDM6A genes in a large cohort of patients with Kabuki syndrome. *Mol. Genet. Metab.*, **107**, 627–629.
32. Greenfield, A., Carrel, L., Pennisi, D., Philippe, C., Quaderi, N., Siggers, P., Steiner, K., Tam, P.P., Monaco, A.P., Willard, H.F. *et al.* (1998) The UTX gene escapes X inactivation in mice and humans. *Hum. Mol. Genet.*, **7**, 737–742.
33. Welstead, G.G., Creyghton, M.P., Bilodeau, S., Cheng, A.W., Markoulaki, S., Young, R.A. and Jaenisch, R. (2012) X-linked H3K27me3 demethylase Utx is required for embryonic development in a sex-specific manner. *Proc. Natl Acad. Sci. USA*, **109**, 13004–13009.
34. Jones, W.D., Dafou, D., McEntagart, M., Woollard, W.J., Elmslie, F.V., Holder-Espinasse, M., Irving, M., Saggar, A.K., Smithson, S., Trembath, R.C. *et al.* (2012) De novo mutations in MLL cause Wiedemann-Steiner Syndrome. *Am. J. Hum. Genet.*, **91**, 358–364.
35. Miyake, N., Tsurusaki, Y., Koshimizu, E., Okamoto, N., Kosho, T., Jane Brown, N., Yang Tan, T., Jia Jiunn Yap, P., Suzumura, H., Tanaka, T. *et al.* (2015) Delineation of clinical features in Wiedemann-Steiner syndrome caused by *KMT2A* mutations: Clinical features in Wiedemann-Steiner syndrome. *Clin. Genet.* 10.1111/cge.12586.
36. Kurotaki, N., Imaizumi, K., Harada, N., Masuno, M., Kondoh, T., Nagai, T., Ohashi, H., Naritomi, K., Tsukahara, M., Makita, Y. *et al.* (2002) Haploinsufficiency of NSD1 causes Sotos syndrome. *Nat. Genet.*, **30**, 365–366.
37. Nimura, K., Ura, K., Shiratori, H., Ikawa, M., Okabe, M., Schwartz, R.J. and Kaneda, Y. (2009) A histone H3 lysine 36 trimethyltransferase links Nkx2–5 to Wolf–Hirschhorn syndrome. *Nature*, **460**, 287–291.
38. Kleefstra, T., Brunner, H.G., Amiel, J., Oudakker, A.R., Nillesen, W.M., Magee, A., Geneviève, D., Cormier-Daire, V., van Esch, H., Fryns, J.-P. *et al.* (2006) Loss-of-function mutations in euchromatin histone methyl transferase 1 (EHMT1) cause the 9q34 subtelomeric deletion syndrome. *Am. J. Hum. Genet.*, **79**, 370–377.
39. Laumonnier, F., Holbert, S., Ronce, N., Faravelli, F., Lenzner, S., Schwartz, C.E., Lespinasse, J., Van Esch, H., Lacombe, D., Goizet, C. *et al.* (2005) Mutations in PHF8 are associated with X linked mental retardation and cleft lip/cleft palate. *J. Med. Genet.*, **42**, 780–786.
40. Vissers, L.E.L.M., van Ravenswaaij, C.M.A., Admiraal, R., Hurst, J. A., de Vries, B.B.A., Janssen, I.M., van der Vliet, W.A., Huys, E.H.L. P.G., de Jong, P.J., Hamel, B.C.J. *et al.* (2004) Mutations in a new member of the chromodomain gene family cause CHARGE syndrome. *Nat. Genet.*, **36**, 955–957.
41. Sanlaville, D. and Verloes, A. (2007) CHARGE syndrome: an update. *Eur. J. Hum. Genet.*, **15**, 389–399.
42. Schnetz, M.P., Bartels, C.F., Shastri, K., Balasubramanian, D., Zentner, G.E., Balaji, R., Zhang, X., Song, L., Wang, Z., LaFramboise, T. *et al.* (2009) Genomic distribution of CHD7 on chromatin tracks H3K4 methylation patterns. *Genome Res.*, **19**, 590–601.
43. Guo, C., Chang, C.C., Wortham, M., Chen, L.H., Kernagis, D.N., Qin, X., Cho, Y.W., Chi, J.-T., Grant, G.A., McLendon, R.E. *et al.* (2012) Global identification of MLL2-targeted loci reveals MLL2's role in diverse signaling pathways. *Proc. Natl Acad. Sci. USA*, **109**, 17603–17608.
44. Holder, N. and Hill, J. (1991) Retinoic acid modifies development of the midbrain-hindbrain border and affects cranial ganglion formation in zebrafish embryos. *Development*, **113**, 1159–1170.
45. Agger, K., Cloos, P.A.C., Christensen, J., Pasini, D., Rose, S., Rappsilber, J., Issaeva, I., Canaani, E., Salcini, A.E. and Helin, K. (2007) UTX and JMJD3 are histone H3K27 demethylases involved in HOX gene regulation and development. *Nature*, **449**, 731–734.
46. Hughes, C.M., Rozenblatt-Rosen, O., Milne, T.A., Copeland, T.D., Levine, S.S., Lee, J.C., Hayes, D.N., Shanmugam, K.S., Bhattacharjee, A., Biondi, C.A. *et al.* (2004) Menin associates with a trithorax family histone methyltransferase complex and with the hoxc8 locus. *Mol. Cell*, **13**, 587–597.
47. Ansari, K.I., Hussain, I., Shrestha, B., Kasiri, S. and Mandal, S.S. (2011) HOXC6 is transcriptionally regulated via coordination of MLL histone methylase and estrogen receptor in an estrogen environment. *J. Mol. Biol.*, **411**, 334–349.
48. Lan, F., Bayliss, P.E., Rinn, J.L., Whetstine, J.R., Wang, J.K., Chen, S., Iwase, S., Alpatov, R., Issaeva, I., Canaani, E. *et al.* (2007) A histone H3 lysine 27 demethylase regulates animal posterior development. *Nature*, **449**, 689–694.
49. Matsumoto, N. and Niikawa, N. (2003) Kabuki make-up syndrome: a review. *Am. J. Med. Genet.*, **117C**, 57–65.
50. Lindgren, A.M., Hoyos, T., Talkowski, M.E., Hanscom, C., Blumenthal, I., Chiang, C., Ernst, C., Pereira, S., Ordulu, Z., Clericuzio, C. *et al.* (2013) Haploinsufficiency of KDM6A is associated with severe psychomotor retardation, global growth restriction, seizures and cleft palate. *Hum. Genet.*, **132**, 537–552.
51. Le Douarin, N.M., Brito, J.M. and Creuzet, S. (2007) Role of the neural crest in face and brain development. *Brain Res. Rev.*, **55**, 237–247.
52. Couly, G.F., Coltey, P.M. and Le Douarin, N.M. (1993) The triple origin of skull in higher vertebrates: a study in quail-chick chimeras. *Development*, **117**, 409–429.

53. Haldeman-Englert, C.R., Chapman, K.A., Kruger, H., Geiger, E.A., McDonald-McGinn, D.M., Rappaport, E., Zackai, E.H., Spinner, B. and Shaikh, T.H. (2010) A de novo 8.8-Mb deletion of 21q21.1-q21.3 in an autistic male with a complex rearrangement involving chromosomes 6, 10, and 21. *Am. J. Med. Genet. A*, **152A**, 196–202.
54. Westerfield, M. (2000) *The Zebrafish Book. A Guide for the Laboratory use of Zebrafish (Danio Rerio)*, 4th edn. Univ. of Oregon Press, Eugene, Oregon.
55. Robu, M.E., Larson, J.D., Nasevicius, A., Beiraghi, S., Brenner, C., Farber, S.A. and Ekker, S.C. (2007) p53 activation by knockdown technologies. *PLoS Genet.*, **3**, e78.
56. Berghmans, S. (2005) tp53 mutant zebrafish develop malignant peripheral nerve sheath tumors. *Proc. Natl Acad. Sci. USA*, **102**, 407–412.
57. Walker, M. and Kimmel, C. (2007) A two-color acid-free cartilage and bone stain for zebrafish larvae. *Biotech. Histochem.*, **82**, 23–28.